General Disclaimer

One or more of the Following Statements may affect this Document

- This document has been reproduced from the best copy furnished by the organizational source. It is being released in the interest of making available as much information as possible.

- This document may contain data, which exceeds the sheet parameters. It was furnished in this condition by the organizational source and is the best copy available.

- This document may contain tone-on-tone or color graphs, charts and/or pictures, which have been reproduced in black and white.

- This document is paginated as submitted by the original source.

- Portions of this document are not fully legible due to the historical nature of some of the material. However, it is the best reproduction available from the original submission.

NATIONAL AERONAUTICS AND SPACE ADMINISTRATION

Technical Memorandum 33-468

Performance of a 20-cm-Diameter Electron-Bombardment Hollow-Cathode Ion Thruster

E. V. Pawlik

JET PROPULSION LABORATORY
CALIFORNIA INSTITUTE OF TECHNOLOGY
PASADENA, CALIFORNIA

February 15, 1971

NATIONAL AERONAUTICS AND SPACE ADMINISTRATION

Technical Memorandum 33-468

Performance of a 20-cm-Diameter Electron-Bombardment Hollow-Cathode Ion Thruster

E. V. Pawlik

JET PROPULSION LABORATORY
CALIFORNIA INSTITUTE OF TECHNOLOGY
PASADENA, CALIFORNIA

February 15, 1971

Prepared Under Contract No. NAS 7-100
National Aeronautics and Space Administration

Preface

The work described in this memorandum was performed by the Propulsion Division of the Jet Propulsion Laboratory.

Contents

Tables

Figures

Abstract

Experimental system studies on solar-electric primary propulsion for deep space probes are presently under way at the Jet Propulsion Laboratory. These studies are performed with a 20-cm-diameter electron-bombardment ion thruster. The electron emitter used to create the thruster plasma has been changed from an oxide to a hollow cathode type in order to improve thruster efficiency and lifetime. The performance of this modified thruster is detailed over a wide range of variations in thruster parameters. Thruster output power can be varied from 1000 to 2600 W.

Performance of a 20-cm-Diameter Electron-Bombardment Hollow-Cathode Ion Thruster

I. Introduction

The application of solar electric primary propulsion is currently of interest for unmanned deep space probes (Refs. 1 and 2). A test program is therefore under way (Refs. 3, 4, and 5) to examine, in detail, the system aspects of this type of propulsion. At the time of initial system studies an oxide cathode was used to provide the source of ionizing electrons within the thruster. Improvements available in cathode lifetime and thruster efficiency have led to the replacement of this cathode with a hollow cathode type (Refs. 6, 7, and 8). This change resulted in several modifications of the original thruster as reported in Ref. 9. The design and performance of the modified thruster is described in this report. This hollow cathode thruster will be incorporated within the ongoing Solar Electric Propulsion System Tests (SEPST) program at JPL.

II. Thruster Design

The basic elements of the present 20-cm-diameter hollow cathode thruster are shown in Figs. 1 and 2. Critical thruster dimensions and materials are indicated on Fig. 2. A weight breakdown for the thruster is presented in Table 1. The front and rear ferromagnetic support rings of the thruster, as indicated on Fig. 2, mount eight bar electromagnets, provide a magnetic flux path, and shape the field within the thruster. The electromagnets consist of two layers of 22-gauge copper wire with a polymide resin insulation (HML) wound on a 0.635-cm diameter cylinder of magnet iron. The insulation meets the thermal service requirements for the NEMA MW-16 specifications.

Two porous tungsten vaporizers were used within the thruster to supply mercury propellant to the hollow

Table 1. Hollow-cathode ion thruster weight summary

Component	Weight, g
Housing	378
Screen grid pole piece	135
Support ring, forward	114
Support ring, aft	128
Anode	200
Rear plate	240
Cathode pole piece and baffle	94
Hollow cathode assembly	180
Cathode vaporizer	28
Screen grid	71
Accelerator grid	525
Magnets (8 each)	600
Accelerator mount assembly (8 each)	220
Ground screen, forward assembly	128
Ground screen, aft assembly	246
Ground screen, back cover	190
Anode and ground screen insulators	40
Mounting ring	300
Connector halves	255
Feed system (vaporizer, insulator & manifold)	100
Total	4072

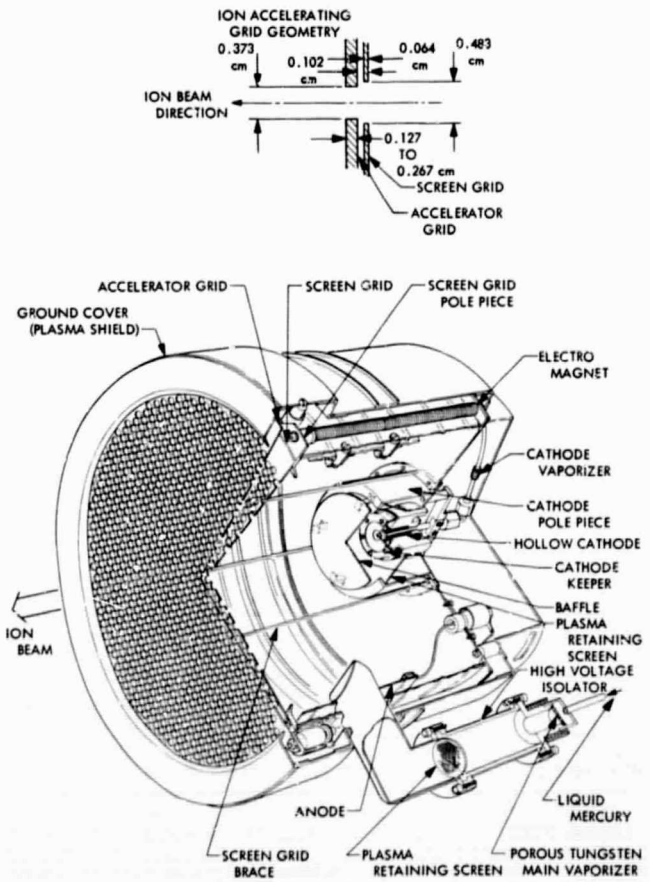

Fig. 1. Cutaway sketch of a 20-cm diameter ion thruster

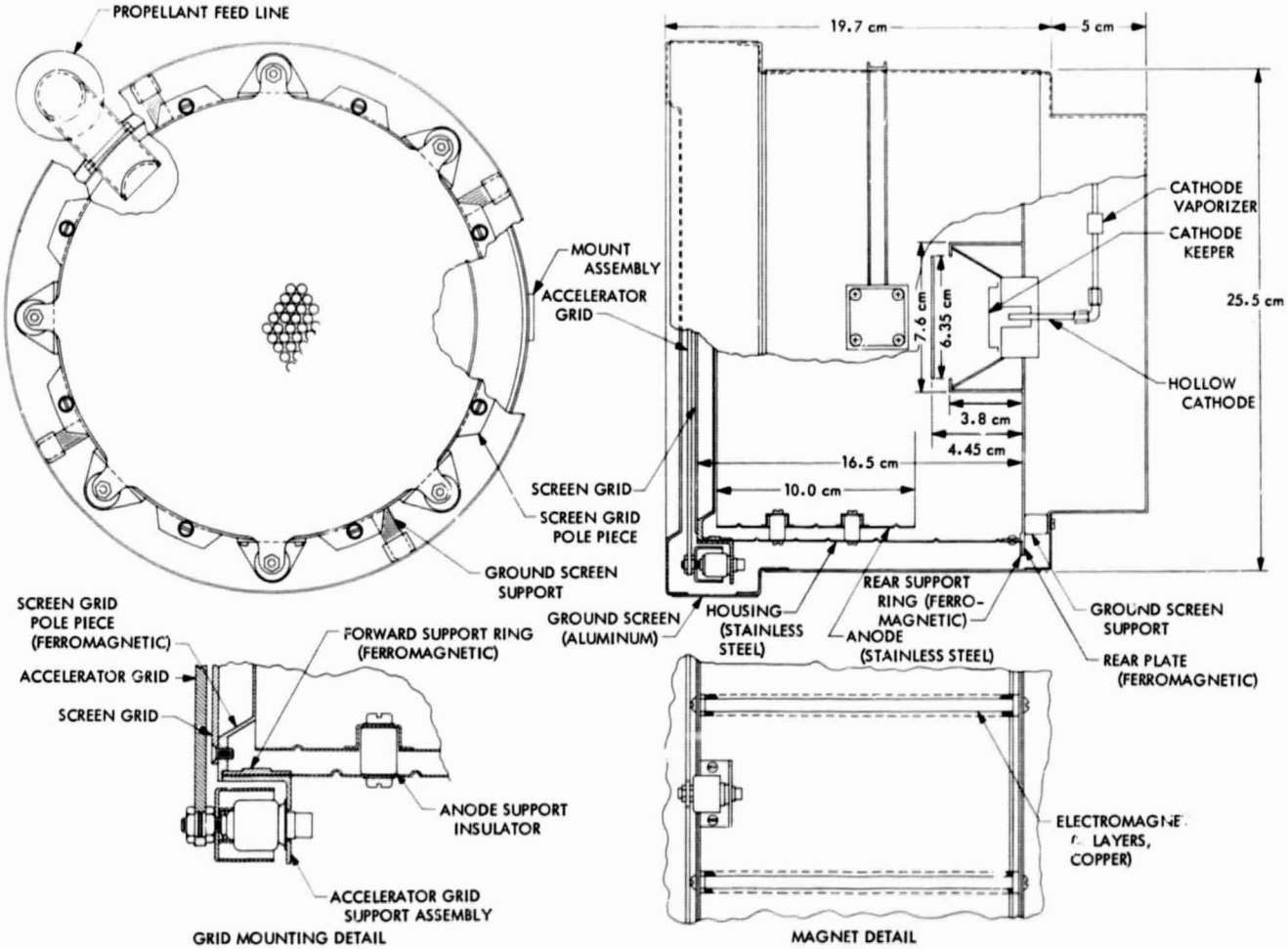

Fig. 2. Thruster design details

cathode and also directly to the arc chamber. The dual vaporizers were desirable because they are more compatible with present thruster control and output power throttling schemes.

Modifications from the thruster design used in the initial system tests (Ref. 9) included: grid geometry changes, screen-grid support rods, replacement of the oxide cathode with a hollow cathode assembly, and a revised thruster mounting arrangement.

A conventional two-grid ion accelerating system was used because of the long experience and proven dependability of this grid type. Tapered accelerator grids were used. The grid thickness decreased with the radial distance from the center of the grid in order to place accelerator material in the region where the greatest wear is generally observed. The center was a constant 0.30 cm thickness to a radius of 5.0 cm, where it decreased uniformly to a thickness of 0.12 cm at the periphery.

The thickness of the screen grid was 0.050 cm. The screen and accelerator hole diameters were 0.482 and 0.373 cm respectively. A 0.075 cm grid separation was maintained. Thin, nonmagnetic, stainless steel rods were attached between the screen grid and the thruster housing. This approach has been found to be desirable (Ref. 4) in limiting the movement of the screen grid as a result of thermal stresses.

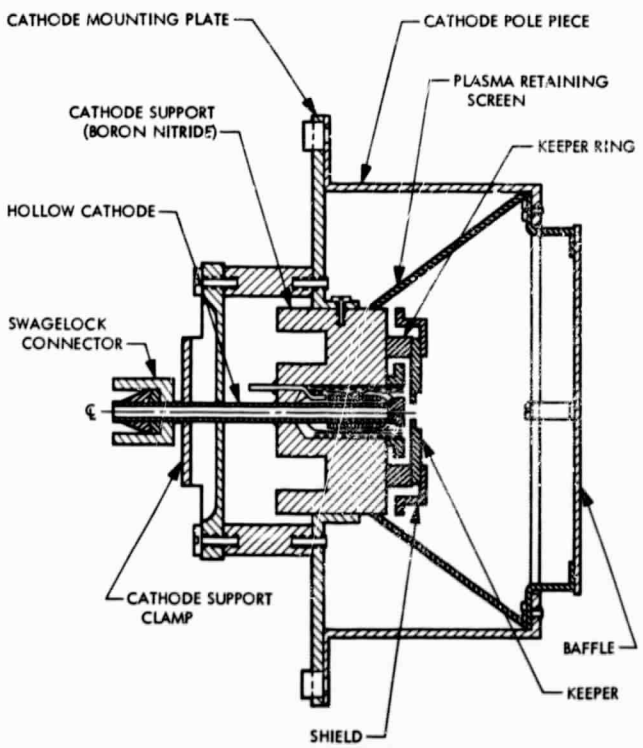

Fig. 3. Hollow-cathode pole piece design details

The thruster mounting was designed to mate with the gimbal elements of the thrust vector alignment system. The actuators for this system are described in Ref. 10. A "C" channel aluminum ring was attached to the thruster cover which was insulated from the thruster and could be electrically grounded. Accurately machined flat surfaces were incorporated at two locations on the ring to define attaching surfaces for bearing mounts.

The details of the hollow cathode assembly as mounted within the cathode pole piece are shown in Fig. 3. An enclosed keeper structure as suggested in Ref. 6 was employed. A plasma retaining screen was incorporated in order to reduce the volume within this structure as suggested by Ref. 11. Mercury flow from the cathode pole piece was directed radially outward by the electron baffle. A similar approach was suggested in Ref. 12 and was found beneficial in reducing accelerator current levels.

III. Thruster Controls

The control loops used to run the thruster while operating on laboratory power supplies are shown in Figs. 4 and 5. The controls presented in Fig. 4 maintain constant mercury flow rates by controlling vaporizer temperatures. This type of control is adequate for most laboratory thruster testing. The control loops presented in Fig. 5 control the mercury flow indirectly by the thruster performance and are presently more suitable for flight operation due to long term drifts that might be expected in the vaporizer temperature-flow calibration.

In the control loops, shown in Fig. 5, the ion beam is compared with a desired operating level generating an error signal to the controller which in turn heats the main propellant vaporizer. The arc voltage is compared against a reference value with the error used to control the heat to the cathode vaporizer. Thruster operation utilizing these loops has been presented in Ref. 13. Thruster output power throttling is accomplished by changing the ion beam current while maintaining the net acceleration voltage constant. Proper thruster operation at each power level is specified by an arc current reference which can be the output of a function generator. The function generator could be programmed for any of several modes of thruster operation such as constant propellant utilization or constant discharge chamber losses.

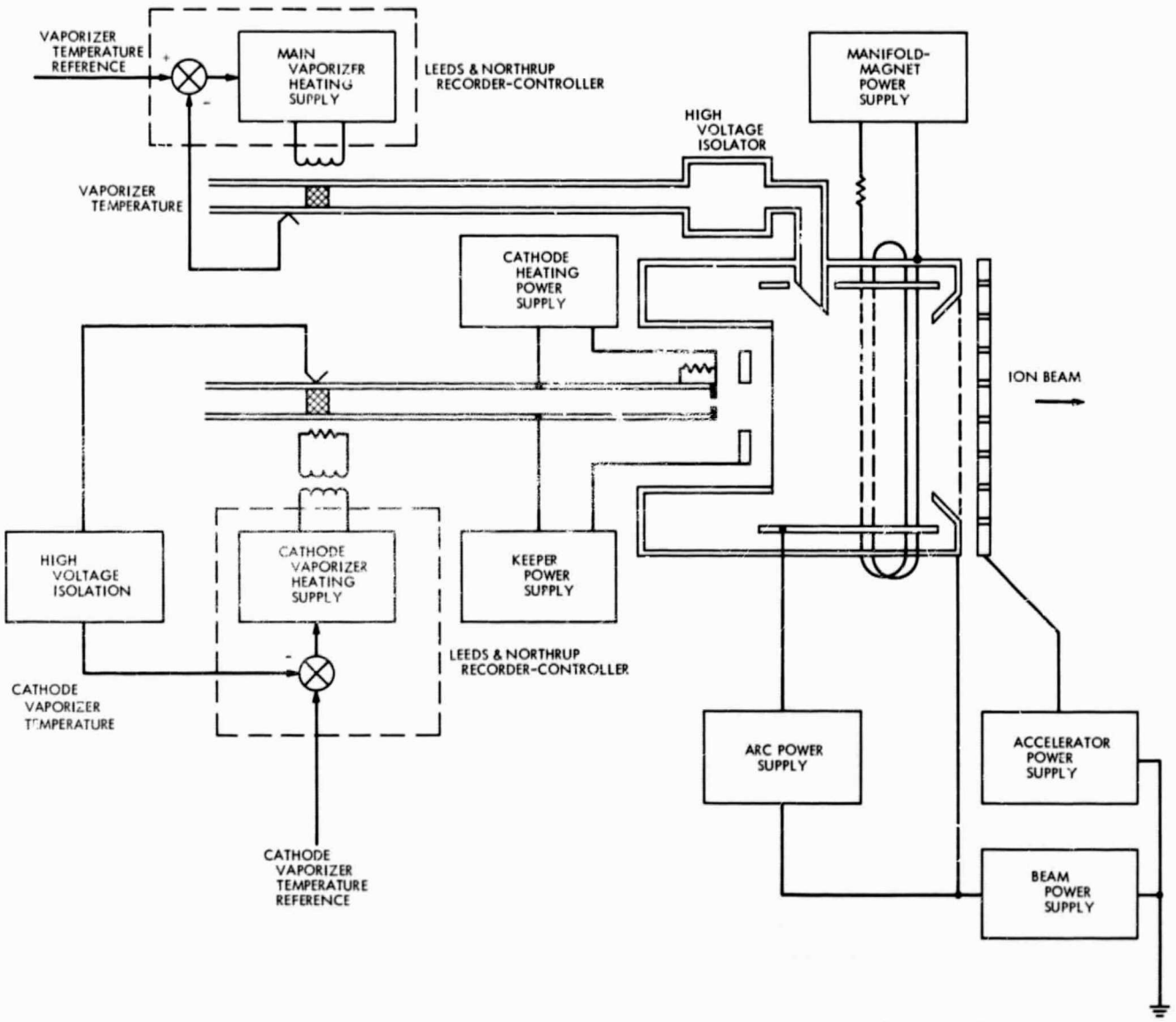

Fig. 4. Power supply schematic and controls, direct vaporizer temperature control

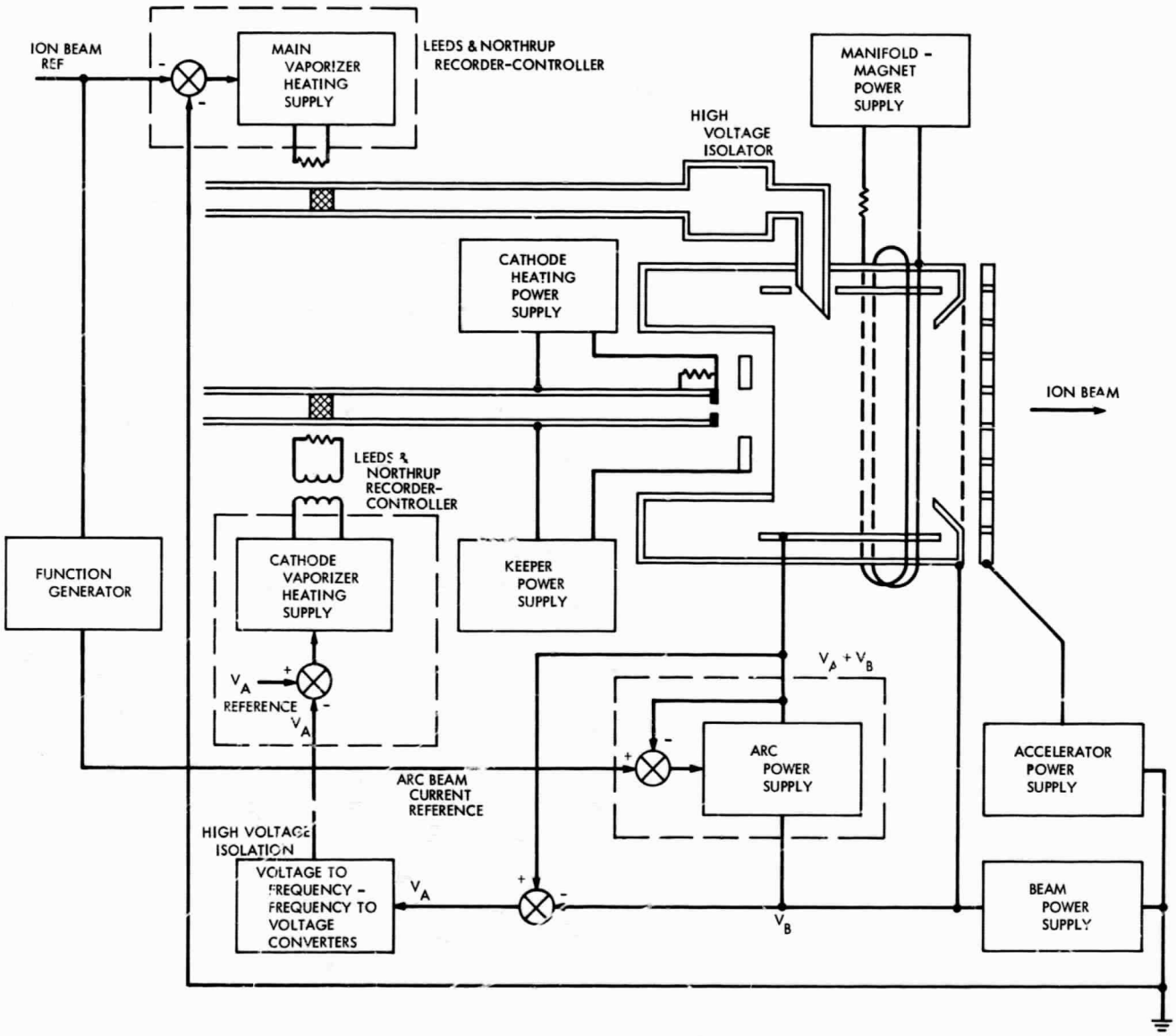

Fig. 5. Power supply schematic and controls, indirect vaporizer temperature control

IV. Thruster Performance

Thruster testing was performed in a vacuum chamber with a diameter of 0.914 m and a length of 2.13 m, maintained at a pressure between 2 to 8 × 10^{-6} torr. The thruster was operated over a range of mercury flow rates that varied between 4.25 to 10.65 g/h (0.57 to 1.42 equivalent amps). Extensive performance data for the thruster was obtained in this flow region. All thruster operation data were obtained with a plasma bridge neutralizer operating. It was located about one meter downstream from the accelerator surface. This was found to be necessary to provide low, steady-state levels of accelerator current. Large and erratic accelerator currents were present when the neutralizer was turned off. The large distance between thruster and neutralizer was chosen so as to minimize the neutralizer ions that might be attracted to the accelerator grid.

The nominal operating levels of the electrical parameters are listed in Table 2. Thruster operation was maintained at an electrical specific impulse of 4450 s. Because of the increased perveance of the ion extraction system, the accelerator voltage was reduced from the 2000 V, used in prior system tests, to 1000 V.

Table 2. Hollow-cathode ion thruster control system electric parameters

Parameter	Current, A	Voltage, V
Accelerator	0.0038–0.0067	1000
Beam	0.500–1.31	2000
Magnet–manifold	0.62	14.0
Cathode heat	1.0	2.4
Cathode keeper	0.4	6.0
Arc	4–10	35.0

The arc chamber losses (arc chamber power per beam ion) are plotted against thruster propellant utilization (ion beam/input mercury flow in amps of Hg^+ equivalent) in Fig. 6. Each initial flowrate was arrived at by adjusting the cathode flow to provide an arc voltage near 35 at a propellant utilization of 90%. The utilization was varied by adjusting the arc current by the current regulation of the arc power supply. The arc voltage usually varied between 30 and 40 V during the mapping. The noise level within the arc current was monitored during this thruster mapping by a high speed strip chart recorder. The noise level, at all flows, increased as the propellant utilization decreased. The noise level usually

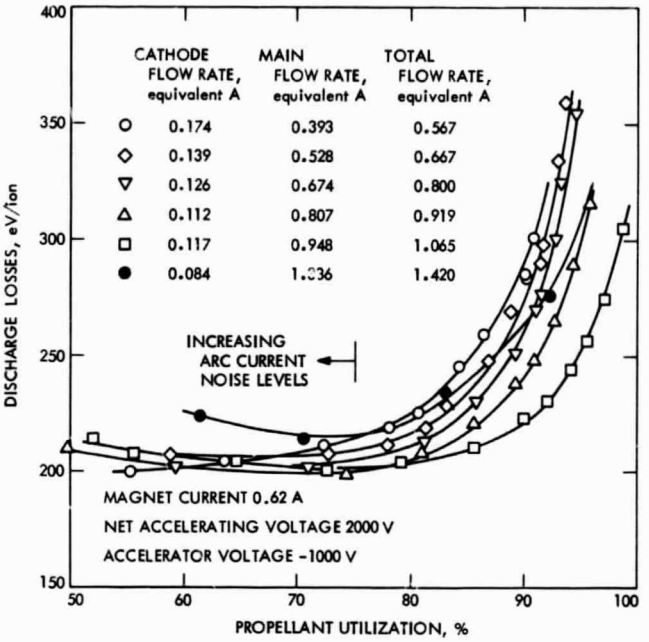

Fig. 6. Effect of propellant flowrate on the discharge loss

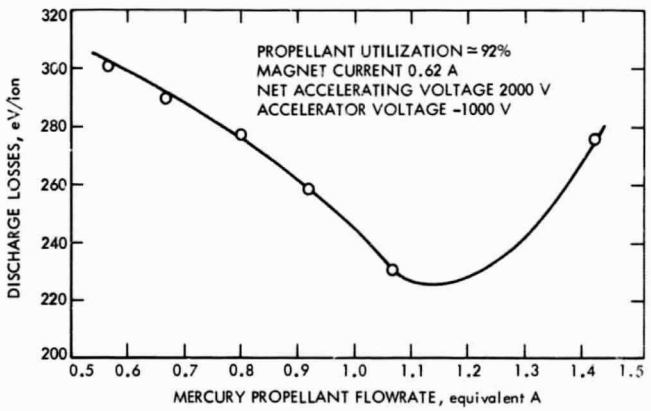

Fig. 7. Effect of propellant flowrate on the discharge loss at constant propellant utilization

became significant (about 3% of the dc level) near a propellant utilization of 75%.

The discharge losses are presented as a function of propellant flow in Fig. 7 for a constant propellant utilization of 90%. The discharge losses for this thruster increased at low propellant flows instead of decreasing as has been observed with oxide cathode thrusters (Ref. 4) or with some hollow cathode thrusters (Ref. 3). This increase results in greater penalties in thruster efficiency when the output power is throttled. Thruster power losses

Table 3. Hollow-cathode ion thruster performance data

Mercury propellant flow rate, equivalent, A	Arc voltage, V	Beam current, A	Beam power, W	Power losses, W					Efficiency, %		
				Arc chamber	Accelerator	Cathode	Magnet-manifold	Main vaporizer	Power	Propellant utilization	Total
0.567	37.73	0.506	1012	152.5	11.1	4.6	8.0	9.9	84.5	90.8	76.7
0.667	36.91	0.610	1220	182.0	9.4	7.1	8.6	10.0	84.8	91.5	77.6
0.800	36.91	0.732	1464	203.0	7.5	9.9	8.5	11.4	85.9	91.6	78.6
0.919	35.17	0.836	1672	208.0	8.9	7.7	8.2	12.5	89.2	91.0	79.4
1.065	34.02	0.980	1960	226.2	12.1	5.7	8.8	11.8	88.1	92.1	81.1
1.420	36.61	1.310	2620	361.1	20.0	4.8	9.3	12.8	86.6	92.3	79.9

and efficiency are presented in Table 3 for a 2.6:1 range in output power near a propellant utilization of 90%.

A map of the thruster performance over a range of output power and propellant utilization is presented in Fig. 8. The data presented in this map was a cross plot of that presented in Fig. 6 with the arc current corrected to an arc voltage of 35 V. This correction assumed constant arc chamber power. The beam and arc voltage are used by the thruster control loops (Fig. 5) to indirectly specify a value of mercury propellant flow rate. It can be seen that specifying the constant values of beam and arc currents to be maintained by these loops uniquely specifies the mercury flow rate only if the propellant utilization remains above 80%.

The variations in accelerator impingement current with thruster parameters are presented in Figs. 9 and 10. The ratio of impingement to beam current as a function of propellant utilization and flowrate is shown in Fig. 9. The ratio was always less than 0.008 at a propellant utilization of 90%. This ratio was highest for low propellant flow rates suggesting a change in the plasma distribution within the arc chamber at these flows. The impingement is presented in Fig. 10 as a function of accelerator voltage and beam current at a propellant utilization in the neighborhood of 90%. The perveance of this grid system was about 8×10^{-6} $A/V^{3/2}$ permitting beam currents of up to 1.3 A without drawing excessive accelerator impingement currents. Thruster operating data were also obtained at closer grid spacing (0.050 cm instead of 0.075 cm) but electron backstreaming of the type observed in Ref. 7 was found to occur frequently.

The effects of variations in the magnetic field on thruster performance and arc chamber voltage are presented in Fig. 11. Data were obtained for constant values of arc current and propellant flow at a nominal one-half and full power thruster operation. The arc voltage and propellant utilization monotonically increased with the magnetic field current. Arc chamber losses were minimal near a magnet current of about 0.5 A. Optimum thruster operation was obtained at the highest magnetic field investigated. However, it appeared to reach a plateau at magnet currents of 0.6 A and above.

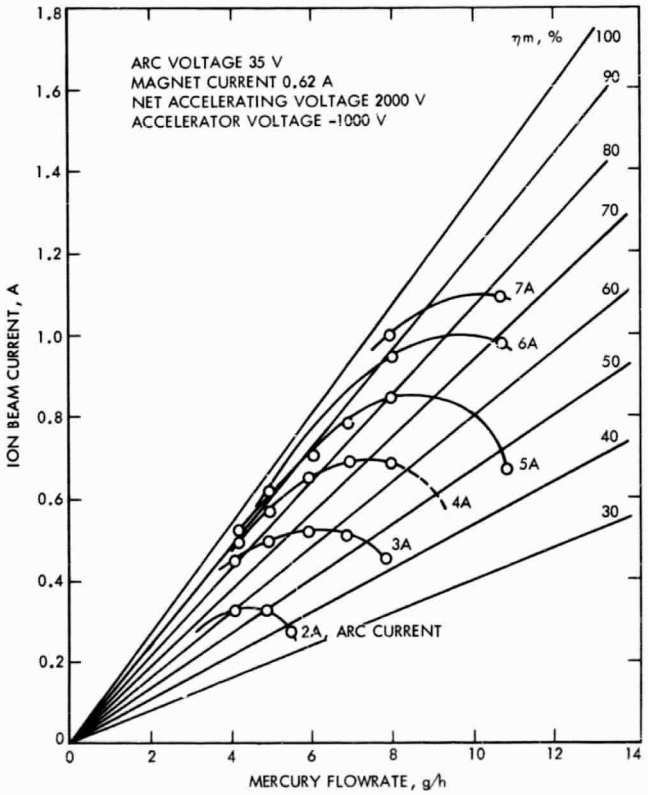

Fig. 8. Cross plot showing effect of propellant flowrate on beam current for constant discharge current

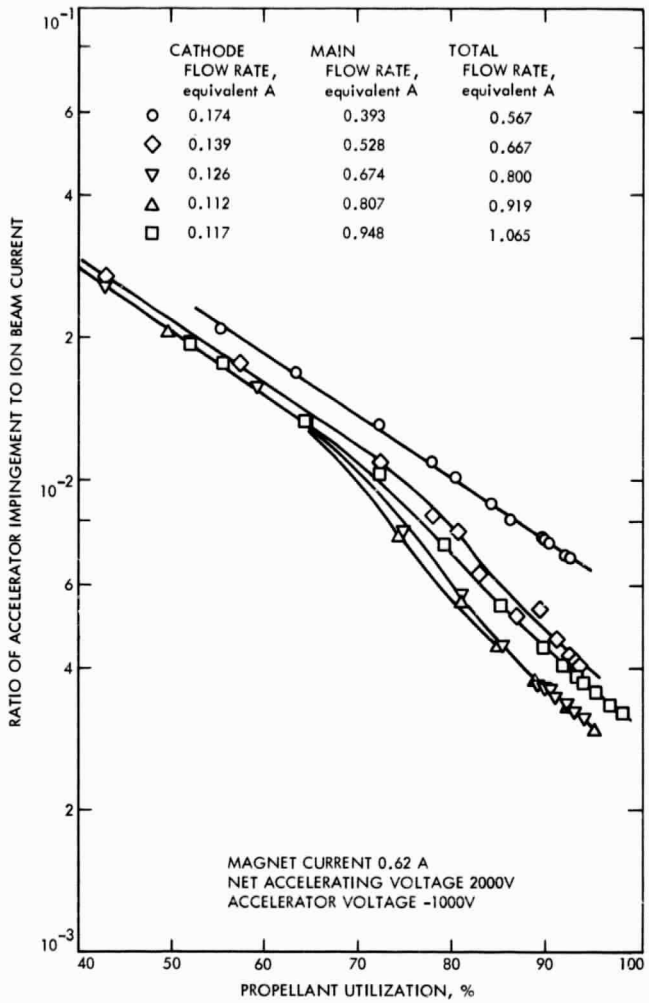

Fig. 9. Effect of propellant flowrate on the impingement to beam current ratio

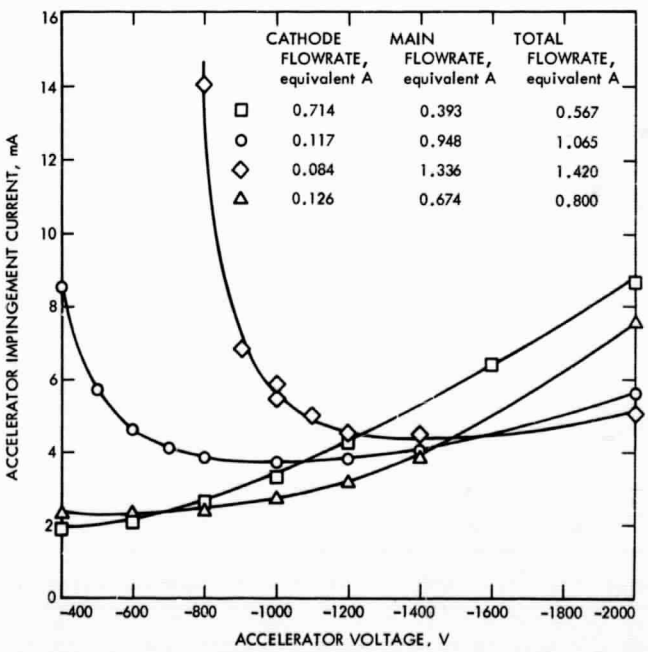

Fig. 10. Effect of accelerator voltage on impingement current

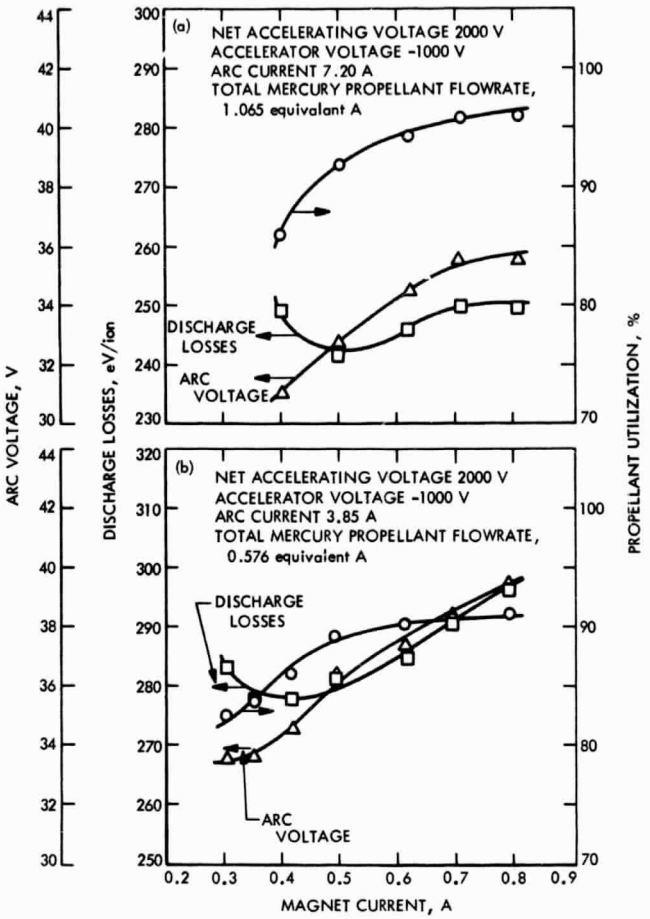

Fig. 11. Effect of magnet current on thruster performance: (a) high propellant flow (1065 mA); (b) low propellant flow (567 mA)

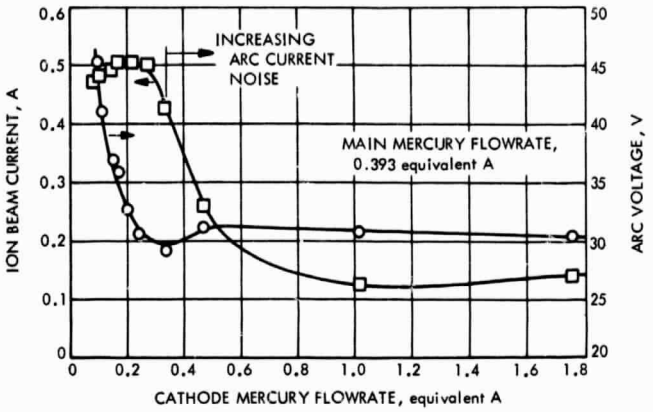

Fig. 12. Effect of cathode mercury flow on thruster performance, low main propellant flow

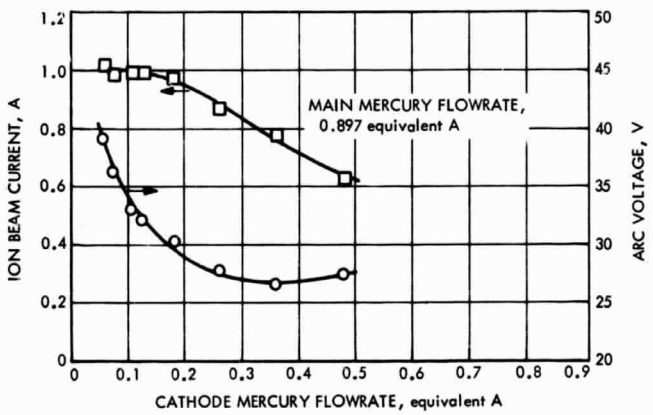

Fig. 13. Effect of cathode mercury flow on thruster performance, high main propellant flow

The level of the arc current noise was also monitored during variations in the magnet current. Intense noise levels were found to exist in the region of magnet current between 0.3 and 0.45 A. The arc discharge extinguished quite often at values of magnet current below 0.3 A, especially at the lower flow rates.

Figures 12 and 13 present the effects of propellant flow through the cathode on thruster operation. Data are again presented for nominal one-half (Fig. 12) and full (Fig. 13) thruster power. The arc voltage and beam currents are plotted in these figures since the cathode flow is used to control the arc voltage directly and can indirectly affect the beam current which is controlled by a second loop. For both main flows the arc could not be maintained below cathode flow rates of 0.3 g/h. As the flow was increased the arc voltage decreased to a minimum value and then increased slightly. Operation at cathode flow rates above that consistent with the minimum arc voltage resulted in increasingly noisy arc current signals.

Most of the above performance data were obtained with the vaporizers being controlled as shown in Fig. 4. The control loops were also connected as shown in Fig. 5 and operated for approximately 8 h intervals at various output power levels between 1000 to 2000 W. The function generator was programmed for constant propellant utilization during these tests. Stable operation was obtained over the 2:1 range of output power.

V. Concluding Remarks

Performance data for a 20-cm-diameter ion thruster employing a hollow cathode have been presented for a wide range of variations in the operating parameters. A

2.6:1 range of output power at a constant propellant utilization of 90% was demonstrated with less than 5% decrease in maximum total efficiency. Thruster operation was well behaved in this region of propellant utilization. Wide excursions in thruster parameters, however, were observed to cause excessive noise levels in the arc current.

A high perveance ion extraction grid system was used. It permitted operation up to 1.3 A of ion beam current at a total acceleration voltage of 3000 V. The current to the accelerator grid was measured at less than 0.8% of the beam current if the thruster was operated at a propellant utilization of 90% or higher.

References

1. *Study of a Solar Electric Multi-Mission Spacecraft*, Final Technical Report, JPL Contract 952394, Document 09451-6001-R0-02. TRW Systems Group, TRW, Inc., Redondo Beach, Calif., Jan. 1970.
2. *Solar Electric Propulsion Asteroid Belt Mission Study*, Final Technical Report, JPL Contract 952566, Document SD-70-21. North American Rockwell Corp., Space Div., Downey, Calif., Jan. 1970.
3. Masek, T. D., and Pawlik, E. V., "Thrust System Technology for Solar Electric Propulsion," Paper 68-541, presented at the AIAA 4th Propulsion Joint Specialist Conference, Cleveland, Ohio, June 1968.
4. Pawlik, E. V., Macie, T. W., and Ferrera, J. D., "Electric Propulsion Systems Performance Evaluation," Paper 69-236, presented at the AIAA 7th Electric Propulsion Conference, Williamsburg, Va., Mar. 1969.
5. Macie, T. W., Pawlik, E. V., Ferrera, J. D., and Costogue, E. N., "Solar-Electric Propulsion System Evaluation," Paper 69-498, presented at the AIAA 5th Propulsion Joint Specialist Conference, U. S. Air Force Academy, Colorado, June 1969.
6. Hall, D. F., Kemp, R. F., and Shelton, H., "Mercury Discharge Devices and Technology," Paper 67-669, presented at the AIAA Conference on Electric Propulsion and Plasmadynamics, Colorado Springs, Colo., Sept. 1967.
7. "Low Specific Impulse Ion Engine," Final Technical Report, NASA Contract NAS3-11523, Hughes Research Laboratories, January 1970.
8. Cisky, G. A., *Investigation of a Hollow Cathode Discharge Plasma*, NASA TM X-52526, National Aeronautics and Space Administration, Washington, 1969.
9. Masek, T. D., "Evaluation of the SE-20C Thruster Design," in *Supporting Research and Advanced Development*, Space Programs Summary 37-51, Vol. III, pp. 124–128. Jet Propulsion Laboratory, Pasadena, Calif., June 30, 1968.

References (contd)

10. Ferrera, J. D., and Perkins, G. S., "Actuator Development for a Clustered Ion Engine Array," in *Supporting Research and Advanced Development*, Space Programs Summary 37-54, Vol. III, pp. 60–63. Jet Propulsion Laboratory, Pasadena, Calif., Dec. 31, 1968.

11. Masek, T. D., "Plasma Properties and Performance of Mercury Ion Thrusters," Paper 69-256, presented at the AIAA 7th Electric Propulsion Conference, Williamsburg, Virginia, Mar. 1969.

12. Masek, T. D., and Womack, J. R., "Hollow Cathode Studies in the SE-20C Ion Thruster," in *Supporting Research and Advanced Development*, Space Programs Summary 37-57, Vol. III, pp. 180–181. Jet Propulsion Laboratory, Pasadena, Calif., June 30, 1969.

13. Pawlik, E. V., and Masek, T. D., "Closed-Loop Operation of a Hollow Cathode Ion Thruster," in *Supporting Research and Advanced Development*, Space Programs Summary 37-60, Vol. III, pp. 206–210. Jet Propulsion Laboratory, Pasadena, Calif., Dec. 31, 1969.

NASA — JPL — Coml., L.A., Calif